



**AFRL-RY-WP-TP-2014-0009**

## **TRANSPARENT CONDUCTING OXIDES FOR INFRARED PLASMONIC WAVEGUIDES: ZnO (PREPRINT)**

**Monica Allen, Jeffery Allen, David Look, and Brett Wenner**

**Electro-Optic Components Branch  
Aerospace Components and Subsystems Division**

**JANUARY 2014**

**Interim**

**Approved for public release; distribution unlimited.**

*See additional restrictions described on inside pages*

**STINFO COPY**

**AIR FORCE RESEARCH LABORATORY  
SENSORS DIRECTORATE  
WRIGHT-PATTERSON AIR FORCE BASE, OH 45433-7320  
AIR FORCE MATERIEL COMMAND  
UNITED STATES AIR FORCE**

# REPORT DOCUMENTATION PAGE

*Form Approved  
OMB No. 0704-0188*

The public reporting burden for this collection of information is estimated to average 1 hour per response, including the time for reviewing instructions, searching existing data sources, gathering and maintaining the data needed, and completing and reviewing the collection of information. Send comments regarding this burden estimate or any other aspect of this collection of information, including suggestions for reducing this burden, to Department of Defense, Washington Headquarters Services, Directorate for Information Operations and Reports (0704-0188), 1215 Jefferson Davis Highway, Suite 1204, Arlington, VA 22202-4302. Respondents should be aware that notwithstanding any other provision of law, no person shall be subject to any penalty for failing to comply with a collection of information if it does not display a currently valid OMB control number. **PLEASE DO NOT RETURN YOUR FORM TO THE ABOVE ADDRESS.**

<b>1. REPORT DATE (DD-MM-YY)</b> January 2014				<b>2. REPORT TYPE</b> Journal Article Preprint				<b>3. DATES COVERED (From - To)</b> 1 August 2012 – 1 August 2013						
<b>4. TITLE AND SUBTITLE</b>  TRANSPARENT CONDUCTING OXIDES FOR INFRARED PLASMONIC WAVEGUIDES: ZnO (PREPRINT)				<b>5a. CONTRACT NUMBER</b> In-house										
				<b>5b. GRANT NUMBER</b> 										
				<b>5c. PROGRAM ELEMENT NUMBER</b> N/A										
<b>6. AUTHOR(S)</b>  Monica Allen, Jeffery Allen, David Look, and Brett Wenner				<b>5d. PROJECT NUMBER</b> N/A										
				<b>5e. TASK NUMBER</b> N/A										
				<b>5f. WORK UNIT NUMBER</b> N/A										
<b>7. PERFORMING ORGANIZATION NAME(S) AND ADDRESS(ES)</b>  Electro-Optic Components Branch Aerospace Components and Subsystems Division Air Force Research Laboratory, Sensors Directorate Wright-Patterson Air Force Base, OH 45433-7320 Air Force Materiel Command, United States Air Force				<b>8. PERFORMING ORGANIZATION REPORT NUMBER</b> AFRL-RY-WP-TP-2014-0009										
				<b>9. SPONSORING/MONITORING AGENCY NAME(S) AND ADDRESS(ES)</b>  Air Force Research Laboratory Sensors Directorate Wright-Patterson Air Force Base, OH 45433-7320 Air Force Materiel Command United States Air Force										
<b>10. SPONSORING/MONITORING AGENCY ACRONYM(S)</b> AFRL/RYDP				<b>11. SPONSORING/MONITORING AGENCY REPORT NUMBER(S)</b> AFRL-RY-WP-TP-2014-0009										
				<b>12. DISTRIBUTION/AVAILABILITY STATEMENT</b> Approved for public release; distribution unlimited.										
<b>13. SUPPLEMENTARY NOTES</b> PAO Case Number 88ABW-2013-3866, Clearance Date 28 August 2013. Paper contains color				<b>14. ABSTRACT</b> Plasmonics combines attractive features of nanoelectronics and optics enabling highly integrated, subwavelength optical and electronic circuits. This review introduces different materials available for plasmonic waveguiding applications with an emphasis on highly conducting ZnO. In addition, the paper contains analysis of a set of thin Al-doped ZnO (AZO) layers grown by RF sputtering on quartz glass that employ a unique, 20-nm-thick, ZnON buffer layer, which minimizes the strong thickness dependence of mobility ( $\mu$ ) on thickness (d).										
<b>15. SUBJECT TERMS</b> microcavity; polariton; strong coupling; ZnO				<b>16. SECURITY CLASSIFICATION OF:</b>										
<b>a. REPORT</b> Unclassified			<b>b. ABSTRACT</b> Unclassified			<b>c. THIS PAGE</b> Unclassified			<b>17. LIMITATION OF ABSTRACT:</b> SAR		<b>18. NUMBER OF PAGES</b> 28		<b>19a. NAME OF RESPONSIBLE PERSON (Monitor)</b> Monica Allen	
<b>19b. TELEPHONE NUMBER (Include Area Code)</b> N/A														

## **Transparent Conducting Oxides for Infrared Plasmonic Waveguides: ZnO**

Monica S. Allen<sup>\*a</sup>, Jeffery W. Allen<sup>\*a</sup>, David C. Look<sup>a,b,c</sup> and Brett R. Wenner<sup>a</sup>

\* These authors have contributed equally to this work

<sup>a</sup> Sensors Directorate, Air Force Research Laboratory, Wright-Patterson AFB, OH 45433

<sup>b</sup> Semiconductor Research Center, Wright State University, Dayton, OH 45435

<sup>c</sup> Wyle Laboratories, Inc., 2601 Mission Point Boulevard, Suite 300, Dayton, OH 45431

**Abstract:** Plasmonics combines attractive features of nanoelectronics and optics enabling highly integrated, subwavelength optical and electronic circuits. Conventional metal-based plasmonic devices have plasmonic resonances less than 1  $\mu\text{m}$ , and thus metals interact effectively only with ultraviolet and visible light. The wide application of plasmonic devices hinges on practical demonstrations with low losses at optical and infrared wavelengths and this field has received much attention in recent years. This review introduces different materials available for plasmonic waveguiding applications with an emphasis on highly conducting ZnO. In addition, the paper contains analysis of a set of thin Al-doped ZnO (AZO) layers grown by RF sputtering on quartz glass that employ a unique, 20-nm-thick, ZnON buffer layer, which minimizes the strong thickness dependence of mobility ( $\mu$ ) on thickness ( $d$ ). The values of mobility and carrier concentration ( $n$ ) were used to predict optical properties through the Drude dielectric function. The optical and electrical properties of the AZO are also used to design insulator-conductor-insulator waveguides for long range plasmons using full-wave electromagnetic models built with finite element method simulations. In many cases, the waveguide has subwavelength dimensions showing that IR light can be manipulated in semiconductor materials at dimensions below the diffraction limit.

**Keywords:** microcavity; polariton; strong coupling; ZnO

### **INTRODUCTION**

The field of plasmonics has received much interest in recent years and several research efforts have been aimed at the understanding of the underlying physics<sup>1</sup>. Recent work has focused on demonstrations that overcome the fabrication and material constraints and enable maturation of the technology into field-testable applications<sup>2</sup> like optical computing and chips, enhanced signal detectors, etc<sup>3</sup>. Surface plasmon polaritons (SPPs) are quasi-particles or excitations that result from resonant coupling of photons to the collective oscillations of conduction electrons in materials<sup>4</sup>. SPPs can be described as two dimensional (2D) bound electromagnetic waves that propagate along conductor-dielectric boundaries<sup>5</sup> and exponentially decay away from this interface<sup>5-7</sup>. These waves are characterized by strongly enhanced localized fields and high spatial confinement, sometimes at subwavelength scales, which makes them attractive for the design of components not constrained by the diffraction limit<sup>8</sup> which may reduce size, weight and power consumption when compared to conventional systems<sup>1,6</sup>.

While the physics behind SPPs was initially explored decades ago, the field has experienced rapid growth in recent years enabled by advances in fabrication techniques which allow for spatial resolution of nanoscale features. Additionally, the refinement of semiconductor processing and exploration of new materials, such as highly conductive semiconductors<sup>9</sup>, has

helped alleviate losses that have hindered the widespread application of conventional metal-based plasmonic devices in the optical and infrared (IR) regime. Recent papers have shown that alternative plasmonic materials such as semiconductor oxides<sup>10-12</sup>, ceramics<sup>13</sup>, semimetals<sup>14</sup>, organics<sup>15</sup> and transition-metal nitrides<sup>16</sup> can offer advantages such as lower losses compared to metals, and tunability of optical properties for different regions of the spectrum including the IR<sup>17,18</sup>.

In this review, we focus on transparent conducting oxides (TCOs) as potential candidates for plasmonic applications in the IR regime. Specifically, we use the example of highly doped ZnO to demonstrate the deposition methods, characterization and simulation of plasmonic waveguides using experimentally measured properties to elucidate the efficacy of these materials in designs where noble metals are the norm. Application of metallic plasmonic devices is relegated to the ultraviolet (UV) and visible (VIS) spectral ranges ( $<1\text{ }\mu\text{m}$ ) since the carrier concentration ( $n$ ) which determines the plasma/resonance frequency ( $\omega_p \propto n^{1/2}$ ) is difficult to change in metals<sup>19,20</sup>. Metals also exhibit large losses in the IR region<sup>21</sup>. Both these issues can be overcome using TCOs e.g. ZnO heavily doped with Al such that  $n > 10^{21}\text{ cm}^{-3}$  translating to a resonant wavelength of approximately  $1\mu\text{m}$  with much lower losses than metals<sup>10,22</sup>.

## PROGRESS HISTORY

Efforts to build plasmonic devices that combine the high bandwidth of photonics with the compactness of electronics<sup>3,23-25</sup> and can be broadly divided into two categories of interest: (i) Sensing applications where local enhancement of electromagnetic (EM) fields using careful design of geometric properties of periodic structures such as metal-hole arrays<sup>26,27</sup> and metal inclusions<sup>23</sup> enables signal-to-noise ratio gains as well as strong nonlinear optical effects<sup>28,29</sup>; and (ii) Light guiding applications where suitable material design and optimized guide geometries can enable confinement of optical modes in subwavelength waveguides<sup>30-32</sup>. This review focusses on waveguides for long-range plasmon excitation and propagation. Traditionally waveguides are made of dielectric media and operate on the principle of light propagation using total internal reflection. The minimum dimension requirement to confine a guided photonic mode is set by the diffraction limit and is typically on the order of  $\lambda_0/n_w$  where  $\lambda_0$  is the wavelength in free space and  $n_w$  is the refractive index of the waveguide. In contrast, plasmonic waveguides can sustain guided modes in subwavelength waveguides using SPPs at conductor-dielectric interfaces<sup>23,33-35</sup>.

Many configurations of SPP waveguides<sup>36</sup> have been proposed to date that leverage characteristics such as mode confinement, and low propagation or coupling losses<sup>37</sup>. They can be broadly classified as metal-insulator-metal (MIM) or insulator-metal-insulator (IMI) waveguides<sup>38-40</sup>. The mode consists of the SPP waves that travel along each of the two dielectric-metal interfaces. A few examples of plasmonic waveguides, comparable to strip waveguides in photonics, are thin metal films<sup>41-43</sup>, cylindrical nanowires<sup>23,44-49</sup>, nanostrips on dielectric substrates<sup>36,38,50,51</sup>, dielectric-loaded SPP waveguides<sup>52-56</sup> and chains of metal nanoparticles<sup>57-60</sup>. Plasmonic waveguides comparable to slot waveguides are nanogaps in thin metal films<sup>24,25,39,61</sup>, channel plasmon polariton waveguides<sup>62-65</sup> and nanogrooves cut in metal media<sup>64-67</sup> e.g. V-grooves<sup>68</sup>, rectangular nanogaps in metallic surrounding films<sup>69-71</sup>, nanoholes in metallic films<sup>25,44</sup> and inverse slots formed by sharp metal wedges<sup>42,64,72,73</sup>. While theoretically plasmonic

waveguide are attractive, each design must be considered for its individual strengths and weaknesses in the context of fabrication constraints and practical imperfections which inevitably diminish predicted performance. For example, nanoholes and nanoparticle chains<sup>74</sup> are difficult to fabricate and exhibit dissipative losses<sup>23</sup>. Strip waveguides<sup>64,75</sup> are easier to fabricate but susceptible to scattering losses due to surface roughness and geometrical aberrations<sup>76</sup>. We consider the hybrid configuration, which aims to combine the tight subdiffraction confinement offered by plasmonic waveguides with longer propagation lengths of dielectric structure<sup>77,78</sup>. This can be constructed by either embedding a conductor waveguide in a dielectric media (IMI) or forming dielectric nanowires coupled to a metal (MIM)<sup>79</sup>. We focus on the IMI hybrid waveguide structure.

The presence of metal in plasmonic waveguides introduces large ohmic losses in the IR regime and has been long considered a major hurdle to wide application of these devices<sup>80</sup>. However, the presence of a conducting medium in the same spatial location as the propagating electric field enables control of mode characteristics<sup>28,52</sup>. In addition, the ability to exercise electrical control in the same waveguide that carries optical information opens the door to many interesting hybrid electro-optical integrated components<sup>81</sup>. Therefore, the best materials for plasmonic components would minimize or eliminate ohmic losses while maintaining the conductivity that allows for the electrical characteristics<sup>19,35</sup>. TCOs may be a good alternative material to implement practical devices that combine these two features.

TCOs have been extensively researched for electrodes and find applications in liquid crystal displays, solar cells and light-emitting diodes<sup>82</sup>. While the most commonly utilized TCO material is indium tin oxide (ITO), its high cost can be prohibitive and a strong candidate to replace ITO is ZnO doped with Al, Ga, or In. Al-doped ZnO (AZO) has also recently been proposed<sup>83</sup> as a plasmonic material in the IR region, a range not accessible to metal-based plasmonics<sup>10,84</sup>. AZO can be easily fabricated into waveguides using standard fabrication techniques e.g. photolithography and patterned into periodic structures such as conductor-hole arrays and nanowire arrays<sup>85-87</sup>. We believe that the material growth techniques and some of the simulations presented for waveguiding applications can be easily extended to periodic arrays for radiation enhancement.

## FABRICATION AND METHODS

ZnO is an attractive material for plasmonic applications because high-quality films can be grown on a variety of substrates using many different methods such as sputtering<sup>88</sup> and pulsed laser deposition (PLD)<sup>89,90</sup>. Material properties can be tuned by controlling carrier concentration ( $n$ ) and, to a lesser extent, mobility ( $\mu$ ). We have recently grown ZnO using PLD and simple air anneals to red-shift the plasmonic resonance to IR wavelengths<sup>10,91</sup>. However, TCO films can have non-uniformities related to growth processes and the non-stoichiometric nature of the materials which causes optical properties to exhibit thickness dependence<sup>92-95</sup>. Further, the substrate interface can have trap states which reduces overall carrier concentration. These losses are thickness dependent due to scattering observed at the microstructure level of the films<sup>89,93</sup>. Another problem with films grown on lattice mismatched substrates is the dependence of electrical properties including resistivity ( $\rho$ ),  $\mu$ , and  $n$ , on the thickness of the film<sup>93,95-97</sup>. It is hypothesized that poor crystallinity near the substrate/film interface gives rise to this problem.

Since uniform thin films with low scattering losses are key to producing practical plasmonic devices, it is not only necessary to understand the origins of thickness dependence of optical properties but also to overcome this issue using careful design of growth processes<sup>98</sup>. Recently, Itagaki et al<sup>99</sup> demonstrated improved crystallinity of RF-sputtered ZnO by inserting a thin ZnON buffer layer between the substrate and ZnO layer. For example, in undoped ZnO grown on c-plane Al<sub>2</sub>O<sub>3</sub>, the rocking-curve FWHM of the (002) diffraction dropped from 0.490° to 0.061°, and in AZO grown on quartz-glass substrates, the thickness dependences of  $\rho$ ,  $\mu$ , and  $n$  was greatly minimized. We also observed low surface roughness and few defects in these films which minimizes losses<sup>97</sup>.

We present results of a set of thin ( $d=25\text{-}147$  nm) AZO layers grown using RF magnetron sputtering at 300°C in 4/20.5 [sccm] N<sub>2</sub>/Ar ambient, producing a total pressure of 0.35 Pa. For each thickness, an AZO film was grown on a bare quartz substrate while another was grown under similar conditions on a substrate with a 20-nm-thick ZnON buffer layer. The targets for the buffers were 99.99% pure ZnO and the applied RF power was 100W. The AZO films were grown at 200°C in pure Ar ambient using ZnO targets with 2wt%Al<sub>2</sub>O<sub>3</sub>. The buffer layers were 20-nm thick, but results not presented here, have shown negligible differences in results for buffer thicknesses from 5-100 nm. Electrically, the buffer layers are semi-insulating with minimal effect on the conductivity of the AZO film. The purpose of the N in the buffer layer is to inhibit the strong nucleation tendency of ZnO, which leads to small grain sizes and results in larger scattering. The buffer increased grain sizes from 38nm to 68nm measured using X-ray diffraction  $\omega\text{-}2\theta$  scans. The buffer also reduces the strong thickness dependence of  $\mu$  and  $n^{100\text{-}102}$ .

## CHARACTERIZATION OF ZnO AS PLASMONIC MATERIAL

Detailed Hall-Effect and reflectance measurements were conducted to quantify the effect of the buffer layer on the quality of the AZO films (Figure 1). Hall-effect measurements were carried out in a LakeShore7507 apparatus. The magnetic field strength was 1T and the temperature range, 6-320 K. The samples were of size 1cm x 1cm, and ohmic indium dots were placed at the four corners. Spectroscopic reflectance measurements were performed in a Perkin-Elmer900 UV/Vis spectrometer at 294K over a wavelength range 190-3200 nm. The volume carrier concentration was independent of thickness and not affected by the buffer. However,  $\mu$  was strongly influenced by the buffer, exhibiting decreased thickness dependence and increased magnitude at a given thickness. The measured data shows that  $n$  does not depend on thickness for either buffered or unbuffered samples nor is it affected by the presence of the buffer. Additionally,  $\mu$  does depend on thickness and is affected by the presence of a buffer. This can be explained by the occurrence of interface scattering where electrons in thinner samples scatter more from the interface because they are closer to it on the average. The buffer reduces this scattering, and also reduces or eliminates the trapping of free electrons from the bulk at the interface<sup>97</sup>.

The measured electrical properties are used to calculate the optical properties of the samples. High carrier concentrations ( $n>10^{20}\text{cm}^{-3}$ ) result in large plasma frequency which in turn results in optical properties akin to Drude metals<sup>22,96,103-105</sup>. Samples of degenerately doped semiconductors like the samples presented here can be described using the Drude function that describes permittivity as a function of frequency (Equation 1). The square root of  $n$  directly

relates to the plasma frequency, and thus the resonance frequency can be easily modified by changing the carrier concentration.

$$\epsilon(\omega) = \epsilon_r + i\epsilon_i = \epsilon_{int} - \frac{\left( \frac{n_{opt}e^2}{\epsilon_0 m^*} \right)}{(\omega^2 + \gamma^2)} + i \frac{\gamma \left( \frac{n_{opt}e^2}{\epsilon_0 m^*} \right)}{\omega(\omega^2 + \gamma^2)} \quad (1)$$

where  $\epsilon_r$  and  $\epsilon_i$  are the real and imaginary part of the permittivity respectively,  $\epsilon_{int}$  is the intrinsic permittivity of the undoped material,  $n_{opt}$  is the optical doping density or carrier concentration,  $\omega$  is the operating frequency,  $e$  is the electron charge,  $m^*$  is the effective mass, and  $\gamma$  is the relaxation rate which can be approximated by  $\gamma = e/\mu_{opt}m^*$  where  $\mu_{opt}$  is the optical mobility. Comparisons of Hall-effect and reflectance measurements in these samples have shown that  $n_{opt} \sim n$ , and  $\mu_{opt} \sim \mu$ . The permittivity calculated using the Drude function is plotted vs. film thicknesses in Figure 2 over a wavelength range of 4-10  $\mu\text{m}$  for both the buffered and unbuffered films.

Both sets of films show similar  $\epsilon_i$  values except at smaller thicknesses where interference scattering comes into play. The buffered films show constant  $\epsilon_i$  even in the thinner samples and the buffer seems to mitigate scattering issues. In the unbuffered samples,  $\epsilon_i$  falls in the thinner samples and this is more pronounced at longer wavelengths. The value of  $\epsilon_r$  varies significantly depending on the presence/absence of the buffer layer but does not change much with thickness in the buffered samples. It increases in magnitude (negative) as wavelength increases but remains almost constant at that value across samples of different thickness in the buffered samples. The biggest variation within these samples is seen at the longest wavelength ( $\lambda=10\mu\text{m}$ ) across thicknesses. Interestingly, this is not the same trend for the unbuffered samples where we observe that the  $\epsilon_r$  is unchanged in the thinner samples irrespective of wavelength but drastically decreases with thickness and the slope of the drop increases with wavelength<sup>97</sup>. This can be attributed to the fact that the mobility in the thinner films for the buffered samples is larger compared to the unbuffered samples and related to lower damping, lower losses and larger crossover frequencies where  $\epsilon_r < 0$ . The permittivity directly affects the analytical dispersion relation and thus the waveguide characteristics such as propagation loss, mode confinement, etc. are dependent on these quantities<sup>106,107</sup>. These values are also used in the EM simulation and thus the electric field associated with each mode, as expected, is affected by the permittivity of the AZO and the surrounding dielectric film.

## DESIGN OF THE PLASMON WAVEGUIDE

Next we demonstrate how the optical properties obtained from the Drude model can be used to design a practical waveguide structure for excitation of long range plasmons, which in many cases supports propagation at the subwavelength scale. The waveguide structure demonstrated here is comparable to the IMI structure in metals<sup>77,108</sup>. The geometry consists of an Insulator-TCO-Insulator where a straight TCO strip waveguide is embedded in a dielectric medium. The structure we analyze is a symmetric slab waveguide structure (Figure 3) consisting of a straight rectangular AZO strip waveguide surrounded by a polymer called benzocyclobutene (BCB) which has a refractive index of ~1.535. The AZO strip has the following dimensions: width=6

$\mu\text{m}$  and thickness ranging from 25-147nm. The AZO film substitutes the metal in the typical IMI setup and the BCB film provides the insulator layer.

Further, the waveguide is a hybrid plasmonic-photonic structure where the electric field travels along the AZO-polymer interface as an SPP mode and the evanescent energy that leaks from the mode is then confined by the dielectric-air boundaries within the larger photonic guide formed by the polymer. This resulting hybrid mode has lower propagation losses than a plasmonic waveguide formed with conductor-air interfaces alone<sup>77</sup>. Plasmonic waveguide geometry and materials can be optimized either to maximize propagation length or confinement to the conductor guide. This trade-off is discussed in greater detail in a later section. Also the operating wavelength is critical to the design since it not only affects the electric field due to the geometry of the waveguide but also because the material parameters (e.g. permittivity) have strong wavelength dependence. This gives the scientist two disparate and uncorrelated design choices that can be adjusted to tailor and optimize the waveguide to best operate for the specific need. The first is the geometry of the device and the second option that is available with TCOs (but not metals) is material parameters by changing doping levels and in turn carrier concentration as well as mobility.

## CHARACTERIZATION OF WAVEGUIDES

The waveguide is analyzed for propagation and confinement properties using an analytical model while the electric field profile is examined using finite element method (FEM) electromagnetic simulations. The values of the material constants for the AZO layer in both sets of models are based on experimental measurements conducted on films that were fabricated by Itagaki et al. The experimental values of mobility and carrier concentration were used in the Drude model of dielectric function to predict the permittivity of the AZO film as a function of wavelength and thickness, which is subsequently used to predict the electric field characteristics using the FEM model and propagating plasmon mode features including losses and confinement using the analytical model.

First we present an analytic model of the waveguide to determine the SPP dispersion, propagation and localization. We assume the films are smooth and lossy with wavelength dependent material parameters derived from experimental measurements. The analytical dispersion results show mode splitting which results in symmetric and antisymmetric field distributions<sup>38</sup>. The analytical solution to the dispersion equation for the TCO film of thickness, d, centered at z=0. The dispersion relations are shown in Equation (2) and (3).

$$L+ : \varepsilon_1 k_{z2} + \varepsilon_2 k_{z1} \tanh\left(\frac{-ik_{z1}d}{2}\right) = 0 \quad (2)$$

$$L- : \varepsilon_1 k_{z2} + \varepsilon_2 k_{z1} \coth\left(\frac{-ik_{z1}d}{2}\right) = 0 \quad (3)$$

where  $k_{z,1,2}^2 = \varepsilon_{1,2} \left(\frac{\omega}{c}\right)^2 - k_x^2$ ,  $k_x = \frac{\omega}{c} \sqrt{\frac{\varepsilon_1 \varepsilon_2}{\varepsilon_1 + \varepsilon_2}}$  and the subscripts 1,2 correspond to the TCO film

and the dielectric medium respectively. Equations (2) and (3) represent coupling modes between

the SPPs and describe the symmetry of the electric field. Equation (2) describes the dispersion relation of the higher energy mode, L+, which is antisymmetric with respect to the z=0 plane. Equation (3), on the other hand, describes the dispersion relation of the lower energy mode, L-, which is symmetric about the z=0 plane<sup>7,38</sup>. The complex wave vectors are calculated using the Eigen value solutions to the wave-vector,  $\beta_0$ , defined by the dispersion relations for wavelengths from  $\lambda=4\text{-}10 \mu\text{m}$ . This IR regime is of interest particularly to enhancing detector signal-to-noise ratio by coupling to plasmonic modes. These quantities were calculated using a 2D unconstrained Nelder-Mead minimization algorithm that used an adaptive simplex method. The minimization criteria used was a tolerance of  $10^{-10} \text{ nm}^{-1}$ . We present simulation results using the analytical as well as EM models for the higher energy mode L+, since the propagation losses for this mode are at least an order of magnitude lower than that of the lower energy mode. The results for L- were also calculated and have the same trends as L+ and hence are not presented in the interest of brevity.

The Eigen value solutions for  $\beta_0$  were used to calculate the real and imaginary part of the effective index for both the buffered and unbuffered samples (Figure 4). The effective index can be represented mathematically as  $n_{\text{eff}} = \beta/k_0$ .  $\beta_0$  and  $k_0$  are propagation constants of the guided wave and wave propagating in free space, respectively. The real part of the effective index is related to the phase delay introduced by the waveguide material per unit length as compared to propagation in vacuum. This quantity also directly affects the confinement of the mode in the waveguide<sup>66</sup>. As the real part of  $n_{\text{eff}}$  increases, the mode is more confined to the AZO waveguide and thus experiences higher losses. The Eigen value solutions for the propagation constant were also used to derive values of propagation length and skin depth.

The optimization of plasmonic waveguides to the specific application of interest hinges on the correct choice of geometrical properties and material parameters that balance the trade-off between propagation length and skin depth which relates to confinement. With this in mind, we compare the performance of the unbuffered and buffered samples of equal thickness at different wavelengths. The propagation characteristics are analyzed using the propagation length (plotted in Figure 5(a)). Propagation length of the plasmonic wave traveling along the conductor-dielectric interface is defined as the 1/e decay length of the electric field, as  $L_{\text{prop}} = 1/[2\text{Im}(\beta)]$ . The decay in the electric field is caused by the ohmic losses of the material which result in loss of energy through heat dissipation<sup>7</sup>.

Next we calculate the skin depth of each waveguide structure as a measure of the confinement of the guide. The SPP electric field skin depth is related to the confinement of the plasmon mode and can be defined as the depth at which the field falls to 1/e in the dielectric medium,  $\delta=1/|k_{zi}|$  where i=1 and 2 correspond to the AZO and the BCB respectively. The extent to which the evanescent field leaks into the dielectric medium, perpendicular to the conductor-dielectric boundary, reveals the confinement of the plasmonic mode within the conductor that makes up the plasmonic waveguide<sup>7</sup>. The skin depth is plotted in Figure 5(b) and the trend is similar for both buffered and unbuffered samples. Skin depth is inversely related to confinement in the TCO film. As skin depth in the dielectric decreases, the electric field is more concentrated in the TCO film and the mode becomes more confined. As expected the trend for skin depth is the same as propagation length. Increased confinement (reduced skin depth) results in greater propagation losses and lower propagation length. Thus, a trade-off has to be made depending on the

application. Further, confinement can be increased at longer wavelengths by optimizing/increasing waveguide width. This is not studied here, since the parameter of interest was thickness and the effect it has on propagation characteristics.

## ELECTROMAGNETIC SIMULATIONS OF THE WAVEGUIDE

The performance of hybrid plasmonic waveguides, such as the one we consider in this paper, depends on both the material properties of the plasmonic waveguide and surrounding dielectric media as well as their geometric dimensions. We study the effect of changing the waveguide properties by using experimentally measured values of material parameters for films with and without a buffer layer and changing the thickness of the waveguide. The Eigen value solutions for the wave vector,  $\beta_0$ , obtained using the analytical model were used to calculate the real and imaginary part of the effective index which was then used as initial guesses in the mode solver in the EM model. The model was parametrically simulated over a mid-IR wavelength range of 4-10 $\mu\text{m}$  and repeated for different film thicknesses with associated mobility and carrier concentration measurements for both the buffered and unbuffered films. The waveguide was simulated using full wave electromagnetic simulations with finite element method (FEM) based software, COMSOL Multiphysics.

The waveguide analyzed in this paper is a symmetric strip waveguide is an AZO strip surrounded by BCB which in turn is surrounded by air for the purpose of simulations. Since the structure is uniform along the length of the device (both in geometry and material), it can be completely characterized using a 2D model of the cross-sectional plane perpendicular to the direction of propagation. This reduces computational overhead and increases speed considerably when compared to a full 3D model. The model is primarily used to analyze the spatial extent of the electric field and profile of the mode with respect to the AZO thin film and the surrounding dielectric. While the mode profile does not change with length, the amplitude of the field decreases to 1/e as the propagation length is approached. We also conducted a frequency domain study to verify the propagation characteristics and those results were found to match the analytical model as expected and are hence not presented. The material characteristics of the AZO waveguide were defined using a Drude model of the complex permittivity as a function of wavelength as described above.

The mesh used in the model consisted of ~64K points over the entire geometry which corresponds to a maximum element size of  $\lambda/8$ . In the regions where the field was expected to rapidly change (e.g. dielectric-conductor boundaries) a finer mesh was used. The computational domain window size was nominally set at 150 $\mu\text{m}$  x 120 $\mu\text{m}$ . The definition of boundary conditions can affect the solution for electric field in plasmon waveguides since the propagating modes are non-radiative and closely bound to its surface. We use scattering boundaries on the outer air boundaries which are placed ~50 $\mu\text{m}$  from the plasmon waveguide at a sufficient distance away such that the plasmonic modes are undisturbed. FEM analysis uses Maxwell's equations in the usual form to calculate the associated electric field mode profiles<sup>106,107</sup>.

These Eigen values derived in the analytical model for each waveguide thickness over the defined wavelength range were used as initial guesses in the mode solver in the finite element simulations. This helps the Eigen solver to converge faster and more accurately to a solution for

the electric field profiles. The Eigen value solutions for the propagation constant were compared to the values obtained in the analytical solution and were found to agree. The results for electric field distribution perpendicular to the direction of propagation are shown in Figure 6 for the buffered samples calculated at  $\lambda=4\mu\text{m}$  for thicknesses ranging from 25-147nm. As the film thickness increases, we notice greater mode confinement in the AZO guide and the evanescent field in the dielectric is minimal. Similar trends and profiles are observed for the unbuffered samples and those results are not presented here.

## CONFINEMENT - PROPAGATION LENGTH TRADE-OFF

SPPs have been researched with respect to different geometries and materials to guide electromagnetic energy at UV/VIS/IR frequencies. The obvious comparison at these frequencies is to dielectric waveguides in terms of performance<sup>109</sup>. Performance can be defined in terms of EM characteristics (propagation length, losses, etc.) and also mechanical properties (size, weight, etc.). Dielectric waveguides confine light in a waveguide core with a higher refractive index than the cladding region when the propagation angle is greater than the critical angle. Plasmonic waveguides, on the other hand, confine electromagnetic energy at the conductor-dielectric interfaces depending on the negative permittivity of the conductor region which acts like the waveguide core. Surface localization in SPPs enables guiding light in structures with dimensions much smaller than their dielectric counterparts, sometimes even subwavelength defying the diffraction limit<sup>23,44,60,106</sup>. This is particularly useful where high density of components<sup>2</sup> with low cross-talk and interference can lead to dramatic improvements in system performance.

SPP propagating modes are concentrated in the conductor core with electric fields formed by the coupling of SPPs at the two metal-dielectric interfaces. This mode coupling reduces losses resulting from the interaction with the conductor but in turn also reduces confinement in both the vertical and lateral dimensions. Propagation lengths of ~2.5mm have been demonstrated for subwavelength waveguides that have confinement in 2D and thin films of finite width with subwavelength confinement in only one dimension have shown propagation lengths over several millimeters<sup>48,50,57</sup>. Tighter confinement of the mode reduces electric field cross-section and causes the fields to be more concentrated to the conductor region which in turn decreases propagation length<sup>37,43,76</sup>. Conversely, allowing the energy to escape into the dielectric medium can alleviate losses but reduces confinement. Thus all plasmonic waveguide configurations must balance the trade-off between confinement and propagation losses and be optimized in accordance with the importance of either in the application<sup>33,68</sup>. This trade-off can be quantified by comparing the dielectric skin depth and propagation length. Tighter confinement to the conductor waveguide is desirable in applications where the mode characteristics may be modified by changing the material characteristics of the guide. This is examined in detail using Figure 7 where the propagation length is plotted with the real part of the effective index which directly relates to confinement and is inversely proportional to dielectric skin depth. As confinement increases, propagation length decreases. This contrasting trend can be balanced using three features, namely width, height and material of the waveguide.

We begin our discussion with the thickness of the guide. Not all the waveguide structures explored for plasmonic mode propagation can be used for subwavelength confinement nor are all supported modes localized in a structure with dimensions under the diffraction limit. Conductor

strip waveguides, like the ones analyzed in this paper, are capable of either short or long range SPP propagation. As seen from the results, reducing film thickness reduces confinement in the conductor and the propagating long range plasmonic modes are weakly localized. These modes are subject to lower losses since only a small portion of the energy is carried in the dissipative conductor while the rest propagates through the lower loss dielectric media. The longer propagation lengths are useful for macroscopic light transport. The hybrid guide can then be used to convert incident light from a dielectric mode (thin conductor) that propagates for several millimeters to an SPP mode (thick conductor) at a specific position along the waveguide to enhance light-matter interaction for applications such as focusing or modulation<sup>110,111</sup>. The SPP mode could then be coupled back to a dielectric mode to transport light to other applications or a detector. Further, the diffused electric field of a dielectric mode can interact effectively with ambient conditions and be used for sensing small changes in refractive index such as those introduced by a target analyte for applications such as chem/bio sensing<sup>112-114</sup>. On the other hand, increasing the thickness of the waveguide increases the localization of the mode. These modes experience high losses and are characterized by lower propagation distances but stronger confinement of the electric field. In strongly confined modes, SPP waveguides can be viewed as light concentrators that enhance light-matter interaction<sup>33,68</sup>. The diminished size of these structures makes them very useful for highly integrated optical circuits and can even be used as subwavelength optical devices in techniques where long propagation lengths are not required to maintain performance.

While the thickness of the waveguide determines confinement in the vertical dimension, the waveguide width can be tailored to alter the mode characteristics in the lateral dimension<sup>75,115</sup>. For a symmetric IMI waveguide constructed of metal, propagation lengths of several microns have been reported for waveguide widths of ~200 nm<sup>45</sup>. As expected, the propagation length depends on the width of the waveguide and previously published results have shown that as the width of the guide decreases, the number of supported modes also falls until a certain width below which no modes are guided<sup>45,75,108,115</sup>. In contrast, waveguides with micrometer widths can support plasmon modes that have propagation lengths of ~1 cm at telecommunication frequencies<sup>116</sup>. This same trend is also observed in asymmetric waveguide structures where the conductor strip is fabricated on an insulating substrate which serves as the lower cladding and air acts as the upper cladding. Although the metal-strip waveguide can, in general, support long propagation lengths for large strip widths, it is not as useful for the purpose of subwavelength confinement.

Finally, the material that constitutes the waveguide can also be altered to either maximize propagation length or confinement as well as add functionality to the device that is not available using metals. The SPP mode can be confined in the z-direction when  $k_z$  is imaginary and  $(\epsilon'_c + \epsilon'_d) < 0$  where  $\epsilon'_c$  and  $\epsilon'_d$  are the permittivity values of the conductor and dielectric respectively. Also,  $\epsilon'_c < 0$  must be satisfied so that  $k_x$  is real and the SPP can propagate in the x-direction. If  $\epsilon'_d = 1$  (air), then  $\epsilon'_c = (\epsilon'_{int} - \epsilon'_{Drude}) < -1$ , where  $\epsilon'_{int}$  is the intrinsic permittivity of the undoped material and  $\epsilon'_{Drude}$  represents the second and third term of equation (1) determined by the material parameters of the conductor. Therefore,  $\epsilon'_{Drude}$  needs to be large ( $\epsilon'_{Drude} = 4.72$  for ZnO) which requires a high carrier concentration coupled with high mobility. High concentration leads to a high refractive index which produces good confinement of the SPP in the conductor with minimal field leakage into the dielectric. On the other hand, high concentration results in greater

losses<sup>10,107</sup>. Plasmonic waveguides are usually made of a noble metal such as silver or gold. The metal layer, which forms a very integral part of plasmonic waveguides, is also responsible for inherent ohmic losses from resistive heating. Metals have very high carrier concentrations and large plasma frequencies which results in high values of imaginary part of permittivity that is responsible for loss<sup>20,38,67</sup>. In addition, practical devices based on metals have imperfections like surface roughness and grain boundaries which increase scattering that also contributes to losses<sup>16,18,21</sup>.

Losses can be mitigated either through loss compensation using gain media or by using lower loss conductors instead of metals<sup>20,117-119</sup>. Some research groups have explored adding optical gain using additional active medium such as pumped dyes in the dielectric layer to compensate for internal, radiative and total losses in the propagating plasmonic waveguide<sup>120-124</sup>. Another approach to lower losses is the use of materials such as transparent conducting oxides or transition metal nitrides which offer a viable alternative in systems where incorporation of gain media may not be easily achieved. Conducting materials such as TCOs can be grown to have appropriate carrier concentrations and thus smaller losses. These materials have demonstrated significantly lower losses when compared to silver, the metal that exhibits the lowest losses in the VIS and near-IR ranges. The growth processes can also be tweaked to reduce losses even more in these alternative materials. For example, nitrides can be deposited as crystalline layers with minimal surface roughness on sapphire which reduces scattering. Another example is the use of a buffer layer (made of ZnON) used with AZO, as discussed in detail in this paper. The N in the buffer layer inhibits the strong nucleation tendency of ZnO, which leads to small grain sizes. X-ray diffraction  $\omega$ -2 $\theta$  scans indicate an increase in grain size from 38 to 68 nm due to the buffer. Further details on growth and structural analysis can be found in Refs xx.

Replacing metals in plasmonic devices also open the door to additional functionality such as static or dynamic tunability. Conventional metals are not tunable and devices have to be designed to work at a specific frequency; therefore, multiple designs are needed for different operating wavelengths, which is not ideal for multispectral application. TCOs and other nitrides allow for tunability and bandgap engineering (e.g., alloying ZnO with Cd and Mg<sup>125</sup>) by changing fabrication processes<sup>126,127</sup>. Furthermore, these materials can be deposited using techniques such as chemical vapor deposition, atomic layer deposition and molecular beam epitaxy which are CMOS-compatible and may lead to integrated monolithic devices.

## CONCLUSIONS

Recent research efforts have focused on the expansion of structures as well as material systems that can be applied in the field of plasmonics. These efforts have led to the successful demonstration of many plasmonic structures that are capable of guiding and manipulating light below the diffraction limit. We reviewed the progress of plasmonic waveguide structures with an emphasis on transparent conducting oxides particularly ZnO as an alternative material for the excitation and propagation of long range plasmons. We also discussed in detail the trade-off presented by plasmonic waveguides between propagation length and confinement and attributes of the waveguide such as choice of materials and geometry that can be used to balance this trade space.

Within this context, we presented simulation results of Al-doped ZnO plasmon waveguide structure surrounded by a dielectric medium that was based on experimentally measured material properties. The permittivity, propagation loss and skin depth of the waveguide were then characterized as a function of Al-doped ZnO film thickness (25-147 nm) and operating wavelength (4-10  $\mu$ m) for films grown both with and without a buffer layer. The buffer layer was shown to be effective in reducing the thickness dependence of material properties of the AZO layers and thus help to improve propagation characteristics. We achieved reasonable values of effective index and a low propagation loss, which verifies that this configuration is suited to the excitation and propagation of long range SPPs in waveguide applications. This indicates that ZnO films grown at different thicknesses with buffer layers still exhibit very similar characteristics in plasmonic waveguide applications. This will help overcome the discrepancy between simulation and experimental results, where fabrication deviations in thickness can create large changes in quality of modes obtained.

The unique ability of plasmonic components<sup>128</sup> to deliver electromagnetic energy via light to both optical and electronic devices makes them attractive for the development of dense integrated optical processing circuits and systems. Since both electrical and optical signals can be transceived using the same structures, plasmonic components will likely provide the link between conventional optical and nanoelectronic components for information and signal processing. The key to practical systems based on plasmonic structures hinges on the development of theoretical<sup>129,130</sup>, fabrication and experimental methods<sup>48</sup> that can reliably and efficiently, generate, manipulate and detect plasmonic waves<sup>131</sup>. Demonstrations of simple plasmonic structures have inspired the recent development of more complicated elements<sup>132</sup> such as resonators<sup>63,133</sup>, interferometers<sup>63</sup>, splitters and integrated active devices<sup>134</sup> that incorporate plasmonics into sources, waveguides and detectors. Plasmonics holds the promise to dramatically improve a wide number of applications such as lab-on-a-chip<sup>116,135</sup>, optical signal processing, sensing and imaging<sup>136</sup>. We believe that plasmonics will enable optical and electronic signal management in unprecedented ways by unifying the most desirable features of electronic and optical devices in novel technology platforms with high performance.

## ACKNOWLEDGMENTS

We wish to thank T.A. Cooper for the Hall-effect measurements, W. Rice for the reflectance measurements, and D. McFarland for technical assistance. The authors are thankful for the funding support through the Air Force Research Laboratory Sensors Directorate. Support of D.C.L. is gratefully acknowledged from the following sources: DOE Grant DE-FG02-07ER46389 (R. Kortan), AFOSR Grant FA9550-10-1-0079 (J. Hwang), NSF Grant DMR-080-3276 (C. Ying), and AFRL Contract HC1047-05-D-4005 (D. Tomich).

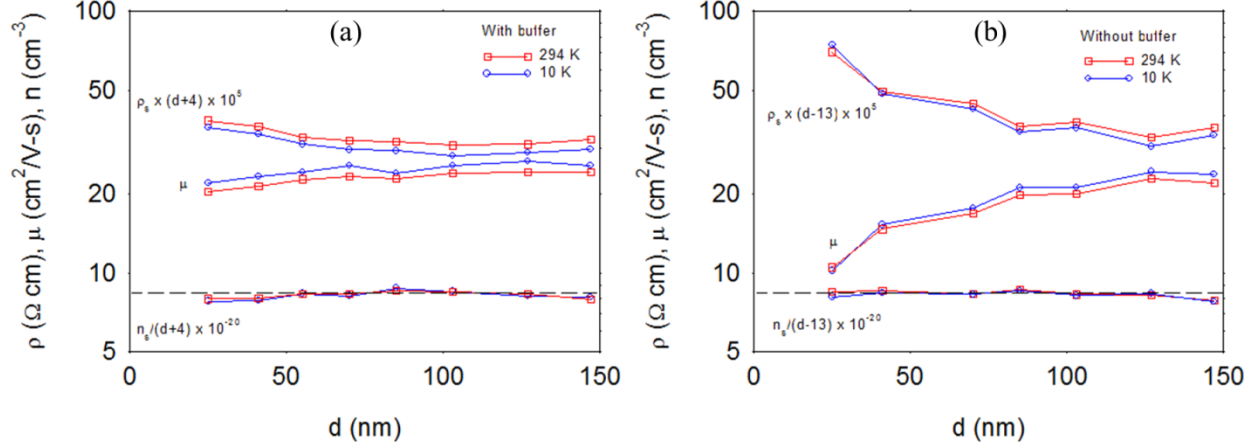


Figure 1: Resistivity ( $\rho$ ), mobility ( $\mu$ ), and carrier concentration ( $n$ ) as a function of film thickness ( $d$ ) for the: (a) Unbuffered samples;  $n$  and  $\rho$  are normalized to electrical thickness,  $d_{el}=d-13$  nm; i.e.,  $n=n_s/(d-13)$ ;  $\rho=\rho_s^*(d-13)$  and (b) Buffered samples;  $n$  and  $\rho$  are normalized to electrical thickness,  $d_{el}=d+4$  nm; i.e.,  $n=n_s/(d+4)$ ;  $\rho=\rho_s^*(d+4)$ . Reprinted from [24].

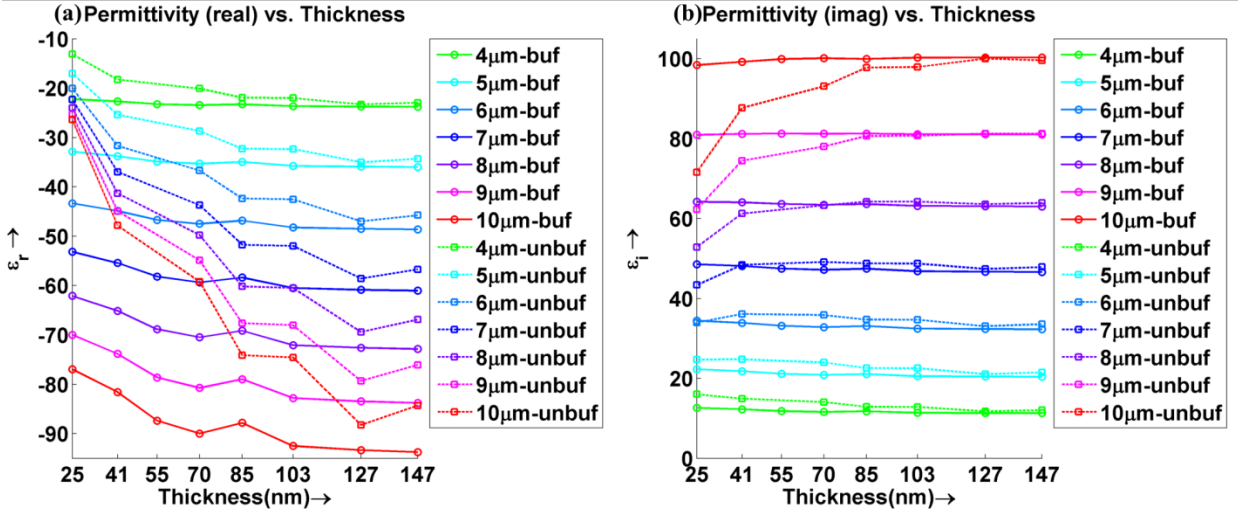


Figure 2: Plot of permittivity ( $\epsilon$ ) vs. waveguide thickness for a symmetric guide with ZnO waveguide embedded in BCB. The different color plots represent each operating wavelength from  $\lambda=4-10\mu m$ . The solid and dashed lines represent the buffered and unbuffered samples respectively.

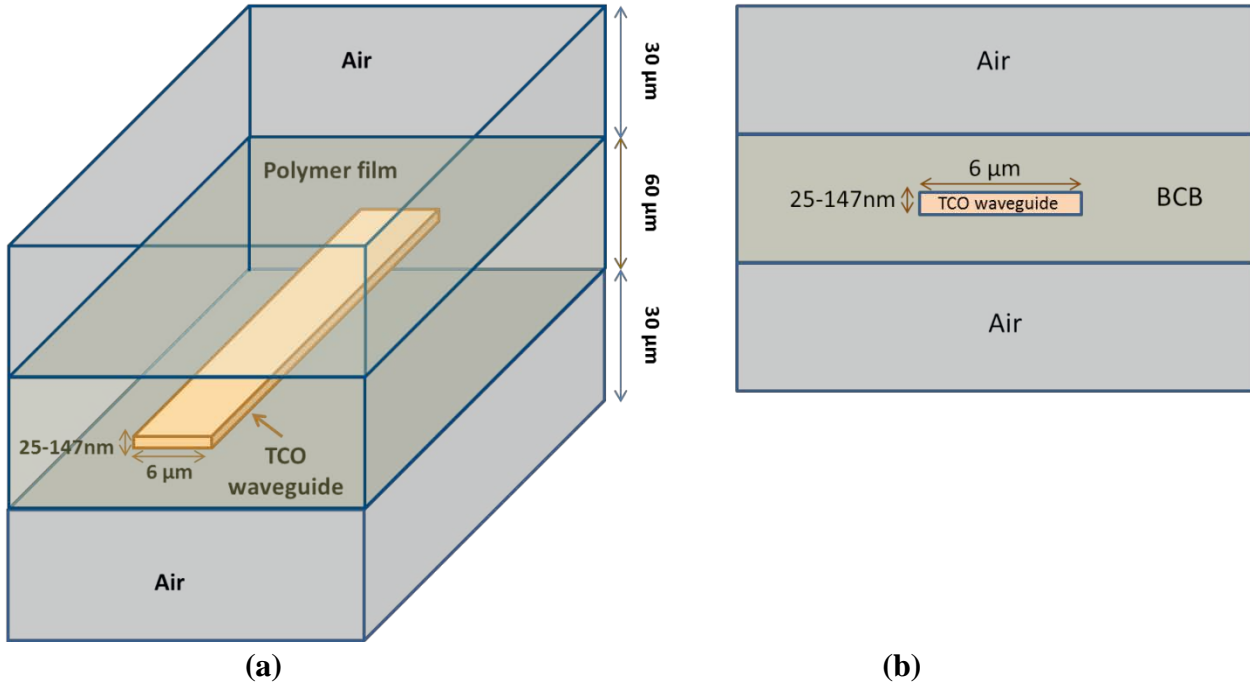


Figure 3: (a) Sketch of the IMI waveguide architecture with quartz substrate, ZnO waveguide and polymer BCB cladding; (b) Waveguide structure in cross-sectional view with dimensions of the guide

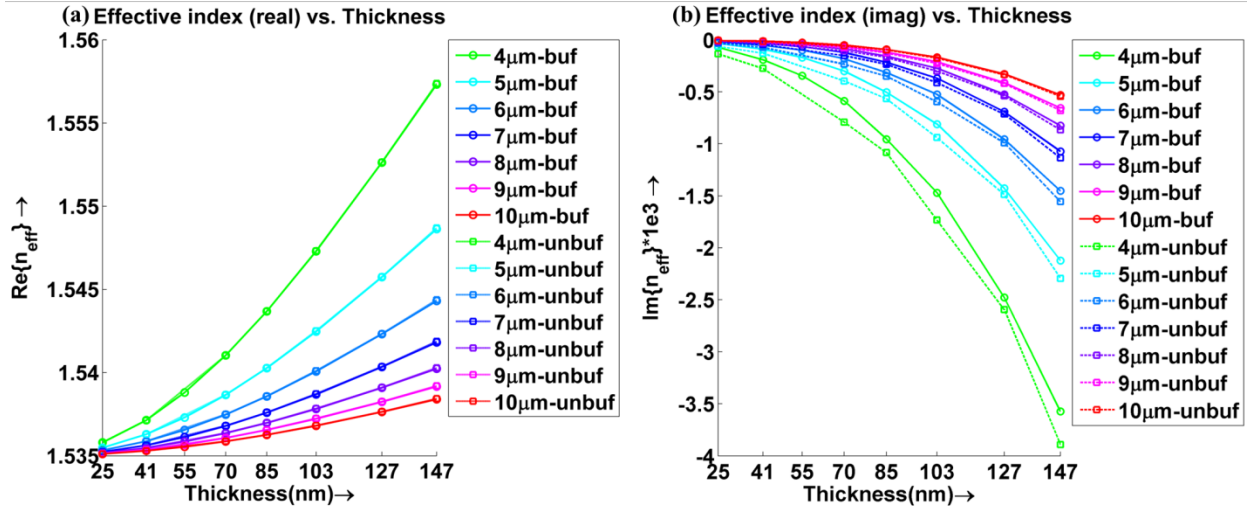


Figure 4: Plot of effective index ( $n_{\text{eff}}$ ) vs. waveguide thickness for a symmetric guide with ZnO waveguide embedded in BCB. The different color plots represent each operating wavelength from  $\lambda=4-10\mu\text{m}$

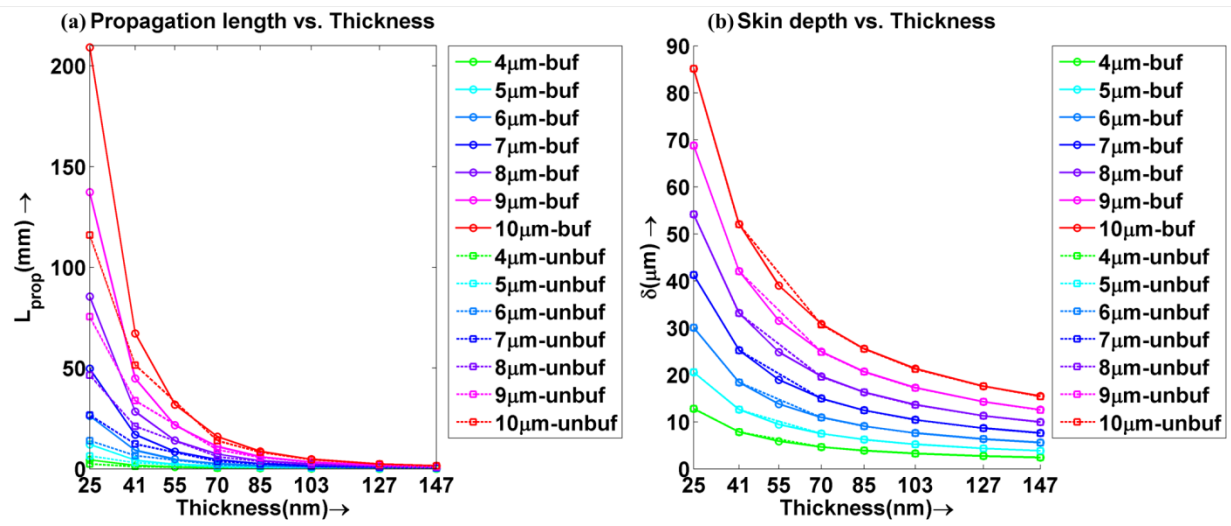


Figure 5: Plot of (a) propagation length ( $L_{\text{prop}}$ ) and (b) skin depth ( $\delta$ ) vs. waveguide thickness for a symmetric guide with quartz substrate, ZnO waveguide embedded in BCB. The different color plots represent each operating wavelength from  $\lambda=4-10\mu\text{m}$

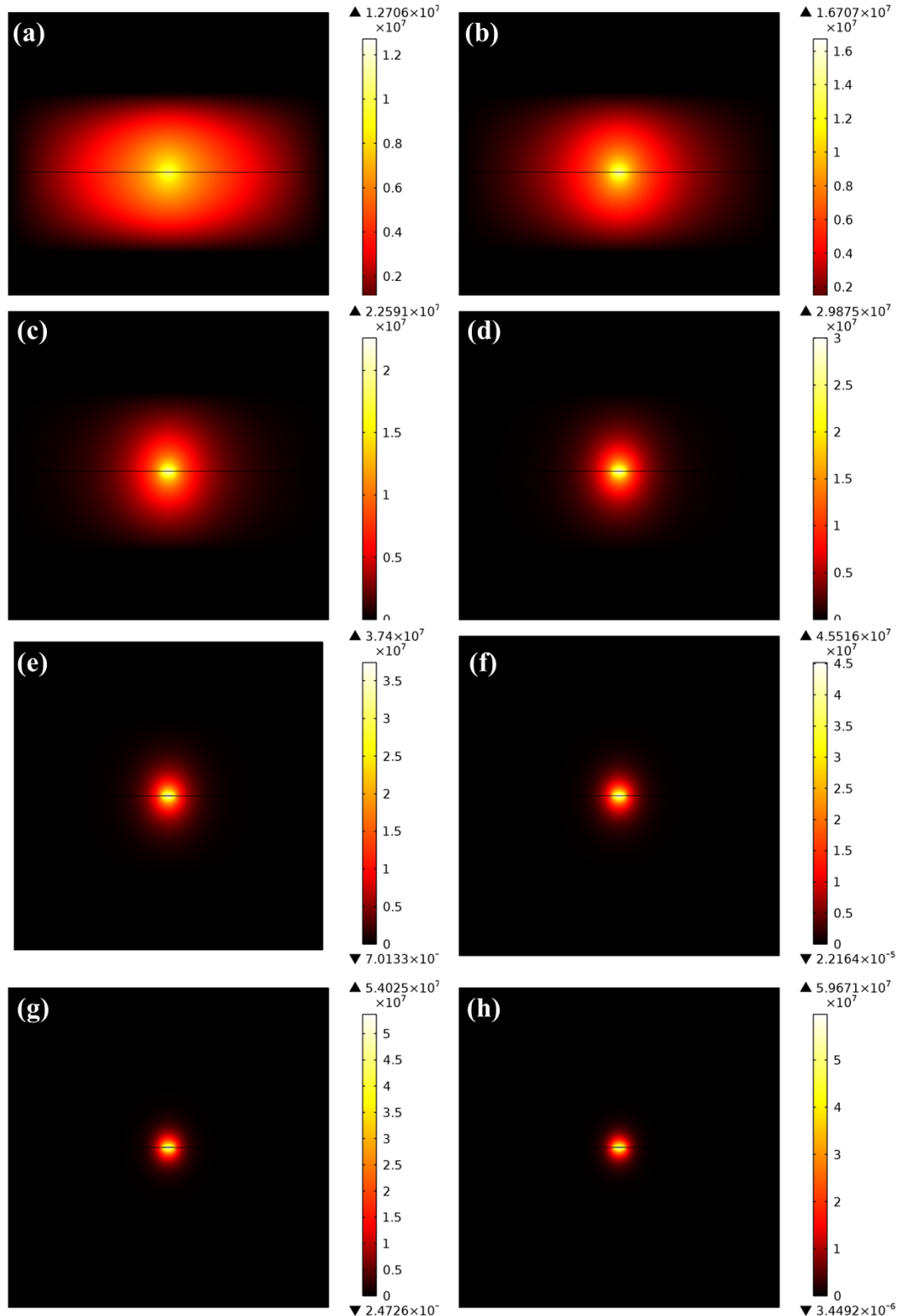


Figure 6: Normalized transverse electric field intensity for symmetric slab insulator-TCO-insulator waveguides at  $\lambda=4\mu\text{m}$  for the buffered samples. Plot of electric field for ZnO waveguide embedded in BCB with ZnO thickness of: (a) 25nm; (b) 41nm; (c) 55nm; (d) 70nm; (e) 85nm; (f) 103nm; (g) 127nm; (h) 147nm

### Prop. length, Eff. index(real) vs. Thickness

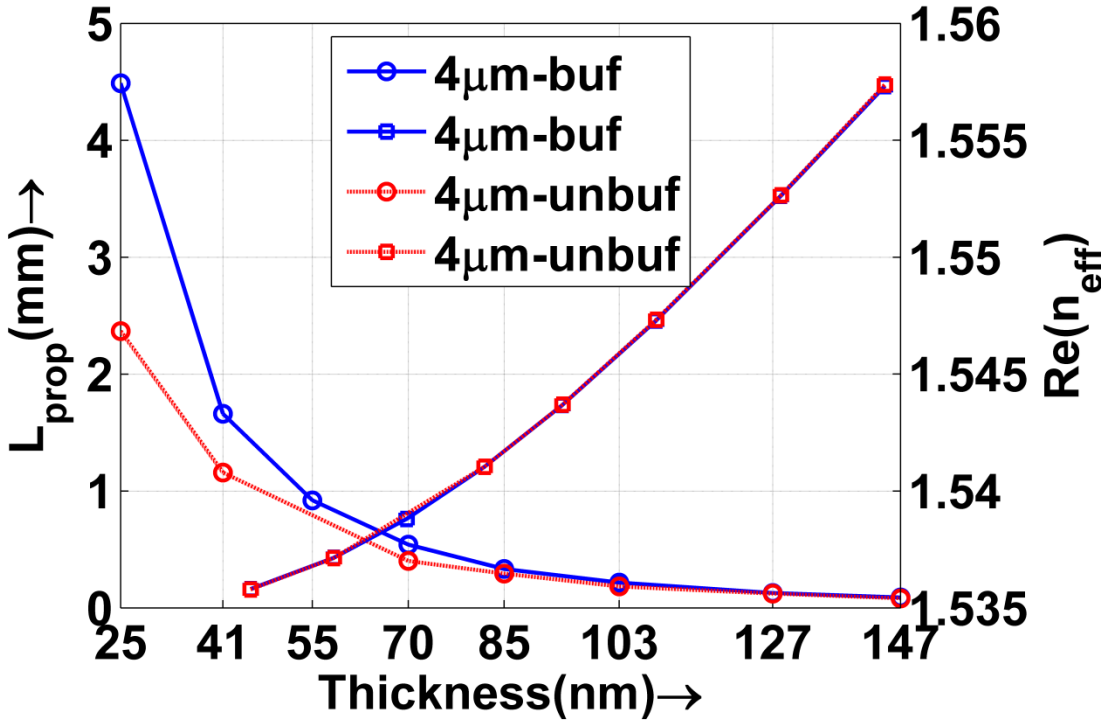


Figure 7: Propagation length ( $L_{prop}$ ) and real part of effective index ( $Re(n_{eff})$ ) vs. waveguide thickness for  $\lambda=4\mu\text{m}$ . The electric field penetrates deeper into the BCB layer as the real part of effective mode index  $Re(n_{eff})$  approaches the refractive index of BCB (1.535). As confinement decreases, propagation length increases.

## REFERENCES

- 1 Barnes, W. L., Dereux, A. & Ebbesen, T. W. Surface plasmon subwavelength optics. *Nature* **424**, 824-830 (2003).
- 2 Kumar, A. *et al.* Dielectric-loaded plasmonic waveguide components: Going practical. *Laser & Photonics Reviews*, n/a-n/a, doi:10.1002/lpor.201200113 (2013).
- 3 Maier, S. A. *et al.* Plasmonics—A Route to Nanoscale Optical Devices (Advanced Materials, 2001, 13, 1501). *Advanced Materials* **15**, 562-562, doi:10.1002/adma.200390134 (2003).
- 4 Ritchie, R. H. Surface plasmons in solids. *Surface Science* **34**, 19 (1973).
- 5 Zayats, A. V., Smolyaninov, I. I. & Maradudin, A. A. Nano-optics of surface plasmon polaritons. *Physics Reports* **408**, 131-314, doi:<http://dx.doi.org/10.1016/j.physrep.2004.11.001> (2005).
- 6 Gramotnev, D. K. & Bozhevolnyi, S. I. Plasmonics beyond the diffraction limit. *Nat Photon* **4**, 83-91 (2010).
- 7 Raether, H. *Surface plasmons on smooth and rough surfaces and gratings*. (Springer-Verlag, 1988).
- 8 Maier, S. A. & Atwater, H. A. Plasmonics: Localization and guiding of electromagnetic energy in metal/dielectric structures. *Journal of Applied Physics* **98**, 011101, doi:10.1063/1.1951057 (2005).
- 9 Hoffman, A. J. *et al.* Negative refraction in semiconductor metamaterials. *Nat Mater* **6**, 946-950, doi:[http://www.nature.com/nmat/journal/v6/n12/supplinfo/nmat2033\\_S1.html](http://www.nature.com/nmat/journal/v6/n12/supplinfo/nmat2033_S1.html) (2007).
- 10 Look, D. C. & Leedy, K. D. ZnO plasmonics for telecommunications. *Applied Physics Letters* **102**, 182107-182104 (2013).
- 11 MacDonald, K. F., Samson, Z. L., Stockman, M. I. & Zheludev, N. I. Ultrafast active plasmonics. *Nat Photon* **3**, 55-58 (2009).
- 12 Noginov, M. A. *et al.* Transparent conductive oxides: Plasmonic materials for telecom wavelengths. *Applied Physics Letters* **99**, 021101-021103 (2011).
- 13 Naik, G. V. & Boltasseva, A. in *CLEO:2011 - Laser Applications to Photonic Applications*. QTuI1 (Optical Society of America).
- 14 Bobb, D. A. *et al.* Engineering of low-loss metal for nanoplasmonic and metamaterials applications. *Applied Physics Letters* **95**, 151102-151103 (2009).
- 15 Zhu, G. *et al.* in *CLEO:2011 - Laser Applications to Photonic Applications*. QThC3 (Optical Society of America).
- 16 Naik, G. V., Kim, J. & Boltasseva, A. Oxides and nitrides as alternative plasmonic materials in the optical range [Invited]. *Opt. Mater. Express* **1**, 1090-1099 (2011).
- 17 Naik, G. V., Shalaev, V. M. & Boltasseva, A. in *Proceedings of SPIE* 7754. 77540M (2010).
- 18 Naik, G. V. & Boltasseva, A. A comparative study of semiconductor-based plasmonic metamaterials. *Metamaterials* **5**, 1-7, doi:<http://dx.doi.org/10.1016/j.metmat.2010.11.001> (2011).
- 19 Boltasseva, A. & Atwater, H. A. Low-Loss Plasmonic Metamaterials. *Science* **331**, 290-291, doi:10.1126/science.1198258 (2011).
- 20 Johnson, P. B. & Christy, R. W. Optical Constants of the Noble Metals. *Physical Review B* **6**, 4370-4379 (1972).

- 21 Naik, G. V. & Boltasseva, A. Semiconductors for plasmonics and metamaterials. *physica status solidi (RRL) – Rapid Research Letters* **4**, 295-297, doi:10.1002/pssr.201004269 (2010).
- 22 Look, D. C., Droubay, T. C. & Chambers, S. A. Optical/electrical correlations in ZnO: The plasmonic resonance phase diagram. *physica status solidi (b)*, n/a-n/a, doi:10.1002/pssb.201200968 (2013).
- 23 Takahara, J., Yamagishi, S., Taki, H., Morimoto, A. & Kobayashi, T. Guiding of a one-dimensional optical beam with nanometer diameter. *Opt. Lett.* **22**, 475-477 (1997).
- 24 Tanaka, K. & Tanaka, M. Simulations of nanometric optical circuits based on surface plasmon polariton gap waveguide. *Applied Physics Letters* **82**, 1158-1160 (2003).
- 25 Tanaka, K., Tanaka, M. & Sugiyama, T. Simulation of practical nanometric optical circuits based on surface plasmon polariton gap waveguides. *Opt. Express* **13**, 256-266 (2005).
- 26 Genet, C. & Ebbesen, T. W. Light in tiny holes. *Nature* **445**, 39-46 (2007).
- 27 Ghaemi, H. F., Thio, T., Grupp, D. E., Ebbesen, T. W. & Lezec, H. J. Surface plasmons enhance optical transmission through subwavelength holes. *Physical Review B* **58**, 6779-6782 (1998).
- 28 Hassan, K., Weeber, J. C., Markey, L. & Dereux, A. Thermo-optical control of dielectric loaded plasmonic racetrack resonators. *Journal of Applied Physics* **110**, 023106-023107 (2011).
- 29 Pacifici, D., Lezec, H. J. & Atwater, H. A. All-optical modulation by plasmonic excitation of CdSe quantum dots. *Nat Photon* **1**, 402-406 (2007).
- 30 Berini, P., Charbonneau, R., Lahoud, N. & Mattiussi, G. Characterization of long-range surface-plasmon-polariton waveguides. *Journal of Applied Physics* **98**, 043109-043112 (2005).
- 31 Steinberger, B. *et al.* Dielectric stripes on gold as surface plasmon waveguides: Bends and directional couplers. *Applied Physics Letters* **91**, 081111-081113 (2007).
- 32 Steinberger, B. *et al.* Dielectric stripes on gold as surface plasmon waveguides. *Applied Physics Letters* **88**, 094104-094103 (2006).
- 33 Berini, P. Plasmon polariton modes guided by a metal film of finite width. *Opt. Lett.* **24**, 1011-1013 (1999).
- 34 Yin, L. *et al.* Subwavelength Focusing and Guiding of Surface Plasmons. *Nano Letters* **5**, 1399-1402, doi:10.1021/nl050723m (2005).
- 35 Nikolajsen, T., Leosson, K. & Bozhevolnyi, S. I. Surface plasmon polariton based modulators and switches operating at telecom wavelengths. *Applied Physics Letters* **85**, 5833-5835 (2004).
- 36 Zia, R., Selker, M. D., Catrysse, P. B. & Brongersma, M. L. Geometries and materials for subwavelength surface plasmon modes. *J. Opt. Soc. Am. A* **21**, 2442-2446 (2004).
- 37 Sarid, D. Long-Range Surface-Plasma Waves on Very Thin Metal Films. *Physical Review Letters* **47**, 1927-1930 (1981).
- 38 Dionne, J. A., Sweatlock, L. A., Atwater, H. A. & Polman, A. Planar metal plasmon waveguides: frequency-dependent dispersion, propagation, localization, and loss beyond the free electron model. *Physical Review B* **72**, 075405 (2005).
- 39 Economou, E. N. Surface Plasmons in Thin Films. *Physical Review* **182**, 539-554 (1969).

- 40 Dionne, J. A., Lezec, H. J. & Atwater, H. A. Highly Confined Photon Transport in Subwavelength Metallic Slot Waveguides. *Nano Letters* **6**, 1928-1932, doi:10.1021/nl0610477 (2006).
- 41 Veronis, G. & Fan, S. Guided subwavelength plasmonic mode supported by a slot in a thin metal film. *Opt. Lett.* **30**, 3359-3361 (2005).
- 42 Pile, D. F. P. *et al.* Two-dimensionally localized modes of a nanoscale gap plasmon waveguide. *Applied Physics Letters* **87**, 261114-261113 (2005).
- 43 Yang, F., Sambles, J. R. & Bradberry, G. W. Long-range surface modes supported by thin films. *Physical Review B* **44**, 5855-5872 (1991).
- 44 Weeber, J.-C., Dereux, A., Girard, C., Krenn, J. R. & Goudonnet, J.-P. Plasmon polaritons of metallic nanowires for controlling submicron propagation of light. *Physical Review B* **60**, 9061-9068 (1999).
- 45 Krenn, J. R. *et al.* Non-diffraction-limited light transport by gold nanowires. *Europhys. Lett.* **60** (2002).
- 46 Chen, X.-W., Sandoghdar, V. & Agio, M. Highly Efficient Interfacing of Guided Plasmons and Photons in Nanowires. *Nano Letters* **9**, 3756-3761, doi:10.1021/nl9019424 (2009).
- 47 Pyayt, A. L., Wiley, B., Xia, Y., Chen, A. & Dalton, L. Integration of photonic and silver nanowire plasmonic waveguides. *Nat Nano* **3**, 660-665 (2008).
- 48 Dickson, R. M. & Lyon, L. A. Unidirectional Plasmon Propagation in Metallic Nanowires. *The Journal of Physical Chemistry B* **104**, 6095-6098, doi:10.1021/jp001435b (2000).
- 49 Sanders, A. W. *et al.* Observation of Plasmon Propagation, Redirection, and Fan-Out in Silver Nanowires. *Nano Letters* **6**, 1822-1826, doi:10.1021/nl052471v (2006).
- 50 Charbonneau, R., Berini, P., Berolo, E. & Lisicka-Shrzek, E. Experimental observation of plasmon polariton waves supported by a thin metal film of finite width. *Opt. Lett.* **25**, 844-846 (2000).
- 51 Verhagen, E., Polman, A. & Kuipers, L. Nanofocusing in laterally tapered plasmonic waveguides. *Opt. Express* **16**, 45-57 (2008).
- 52 Gosciniak, J. *et al.* Thermo-optic control of dielectric-loaded plasmonic waveguide components. *Opt. Express* **18**, 1207-1216 (2010).
- 53 Holmggaard, T. & Bozhevolnyi, S. I. Theoretical analysis of dielectric-loaded surface plasmon-polariton waveguides. *Physical Review B* **75**, 245405 (2007).
- 54 Holmggaard, T., Bozhevolnyi, S. I., Markey, L. & Dereux, A. Dielectric-loaded surface plasmon-polariton waveguides at telecommunication wavelengths: Excitation and characterization. *Applied Physics Letters* **92**, 011124-011123 (2008).
- 55 Hohenau, A. *et al.* Dielectric optical elements for surface plasmons. *Opt. Lett.* **30**, 893-895 (2005).
- 56 Reinhardt, C. *et al.* Laser-fabricated dielectric optical components for surface plasmon polaritons. *Opt. Lett.* **31**, 1307-1309 (2006).
- 57 Maier, S. A. *et al.* Local detection of electromagnetic energy transport below the diffraction limit in metal nanoparticle plasmon waveguides. *Nature Materials* **2**, 229-232 (2003).
- 58 Maier, S. A., Brongersma, M. L., Kik, P. G. & Atwater, H. A. Observation of near-field coupling in metal nanoparticle chains using far-field polarization spectroscopy. *Physical Review B* **65**, 193408 (2002).

- 59 Maier, S. A., Kik, P. G. & Atwater, H. A. Observation of coupled plasmon-polariton modes in Au nanoparticle chain waveguides of different lengths: Estimation of waveguide loss. *Applied Physics Letters* **81**, 1714-1716 (2002).
- 60 Quinten, M., Leitner, A., Krenn, J. R. & Ausseneegg, F. R. Electromagnetic energy transport via linear chains of silver nanoparticles. *Opt. Lett.* **23**, 1331-1333 (1998).
- 61 Wang, B. & Wang, G. P. Surface plasmon polariton propagation in nanoscale metalgap waveguides. *Opt. Lett.* **29**, 1992-1994 (2004).
- 62 Bozhevolnyi, S. I., Volkov, V. S., Devaux, E. & Ebbesen, T. W. Channel Plasmon-Polariton Guiding by Subwavelength Metal Grooves. *Physical Review Letters* **95**, 046802 (2005).
- 63 Bozhevolnyi, S. I., Volkov, V. S., Devaux, E., Laluet, J.-Y. & Ebbesen, T. W. Channel plasmon subwavelength waveguide components including interferometers and ring resonators. *Nature* **440**, 508-511 (2006).
- 64 Moreno, E., Garcia-Vidal, F. J., Rodrigo, S. G., Martin-Moreno, L. & Bozhevolnyi, S. I. Channel plasmon-polaritons: modal shape, dispersion, and losses. *Opt. Lett.* **31**, 3447-3449 (2006).
- 65 Novikov, I. V. & Maradudin, A. A. Channel polaritons. *Physical Review B* **66**, 035403 (2002).
- 66 Lee, I.-m., Jung, J., Park, J., Kim, H. & Lee, B. Dispersion characteristics of channel plasmon polariton waveguides with step-trench-type grooves. *Opt. Express* **15**, 16596-16603 (2007).
- 67 Gramotnev, D. K. & Pile, D. F. P. Single-mode subwavelength waveguide with channel plasmon-polaritons in triangular grooves on a metal surface. *Applied Physics Letters* **85**, 6323-6325 (2004).
- 68 Berini, P. Plasmon-polariton waves guided by thin lossy metal films of finite width: Bound modes of symmetric structures. *Physical Review B* **61**, 10484-10503 (2000).
- 69 Dionne, J. A., Sweatlock, L. A., Atwater, H. A. & Polman, A. Plasmon slot waveguides: Towards chip-scale propagation with subwavelength-scale localization. *Physical Review B* **73**, 035407 (2006).
- 70 Neutens, P., Van Dorpe, P., De Vlaminck, I., Lagae, L. & Borghs, G. Electrical detection of confined gap plasmons in metal-insulator-metal waveguides. *Nat Photon* **3**, 283-286 (2009).
- 71 Veronis, G. & Shanhui, F. Modes of Subwavelength Plasmonic Slot Waveguides. *Lightwave Technology, Journal of* **25**, 2511-2521, doi:10.1109/jlt.2007.903544 (2007).
- 72 Nerkararyan, K. V. Superfocusing of a surface polariton in a wedge-like structure. *Physics Letters A* **237**, 103-105, doi:[http://dx.doi.org/10.1016/S0375-9601\(97\)00722-6](http://dx.doi.org/10.1016/S0375-9601(97)00722-6) (1997).
- 73 Boltasseva, A. *et al.* Triangular metal wedges for subwavelengthplasmon-polariton guiding at telecomwavelengths. *Opt. Express* **16**, 5252-5260 (2008).
- 74 Futamata, M., Maruyama, Y. & Ishikawa, M. Local Electric Field and Scattering Cross Section of Ag Nanoparticles under Surface Plasmon Resonance by Finite Difference Time Domain Method. *The Journal of Physical Chemistry B* **107**, 7607-7617, doi:10.1021/jp022399e (2003).
- 75 Lamprecht, B. *et al.* Surface plasmon propagation in microscale metal stripes. *Applied Physics Letters* **79**, 51-53 (2001).

- 76 Burke, J. J., Stegeman, G. I. & Tamir, T. Surface-polariton-like waves guided by thin, lossy metal films. *Physical Review B* **33**, 5186-5201 (1986).
- 77 Degiron, A. *et al.* Simulations of hybrid long-range plasmon modes with application to 90° bends. *Opt. Lett.* **32**, 2354-2356 (2007).
- 78 Oulton, R. F., Sorger, V. J., Genov, D. A., Pile, D. F. P. & Zhang, X. A hybrid plasmonic waveguide for subwavelength confinement and long-range propagation. *Nat Photon* **2**, 496-500, doi:[http://www.nature.com/nphoton/journal/v2/n8/suppinfo/nphoton.2008.131\\_S1.html](http://www.nature.com/nphoton/journal/v2/n8/suppinfo/nphoton.2008.131_S1.html) (2008).
- 79 Welford, K. R. & Sambles, J. R. Coupled Surface Plasmons in a Symmetric System. *Journal of Modern Optics* **35**, 1467-1483, doi:10.1080/09500348814551611 (1988).
- 80 Podolskiy, V. A., Sarychev, A. K. & Shalaev, V. M. Plasmon modes in metal nanowires and left-hand materials. *Journal of Nonlinear Optical Physics and Materials* **11**, 65-74 (2002).
- 81 Ebbesen, T. W., Genet, C. & Bozhevolnyi, S. I. Surface-plasmon circuitry. *Physics Today* **61**, 44-50 (2008).
- 82 Ozgur, U. *et al.* A comprehensive review of ZnO materials and devices. *Journal of Applied Physics* **98**, 041301-041103 (2005).
- 83 Gâlcă, A. C., Secu, M., Vlad, A. & Pedarnig, J. D. Optical properties of zinc oxide thin films doped with aluminum and lithium. *Thin Solid Films* **518**, 4603-4606, doi:<http://dx.doi.org/10.1016/j.tsf.2009.12.041> (2010).
- 84 Ellmer, K. & Mientus, R. Carrier transport in polycrystalline ITO and ZnO:Al II: The influence of grain barriers and boundaries. *Thin Solid Films* **516**, 5829-5835, doi:<http://dx.doi.org/10.1016/j.tsf.2007.10.082> (2008).
- 85 Garry, S., McCarthy, E., Mosnier, J. P. & McGlynn, E. Control of ZnO nanowire arrays by nanosphere lithography (NSL) on laser-produced ZnO substrates. *Applied Surface Science* **257**, 5159-5162, doi:<http://dx.doi.org/10.1016/j.apsusc.2010.11.182> (2011).
- 86 Liu, D. F. *et al.* Periodic ZnO Nanorod Arrays Defined by Polystyrene Microsphere Self-Assembled Monolayers. *Nano Letters* **6**, 2375-2378, doi:10.1021/nl061399d (2006).
- 87 Ng, H. T. *et al.* Optical properties of single-crystalline ZnO nanowires on m-sapphire. *Applied Physics Letters* **82**, 2023-2025 (2003).
- 88 Tominaga, K. *et al.* 3 edn 1074-1079 (AVS).
- 89 Kim, H., Horwitz, J. S., Qadri, S. B. & Chrisey, D. B. Epitaxial growth of Al-doped ZnO thin films grown by pulsed laser deposition. *Thin Solid Films* **420-421**, 107-111, doi:[http://dx.doi.org/10.1016/S0040-6090\(02\)00658-2](http://dx.doi.org/10.1016/S0040-6090(02)00658-2) (2002).
- 90 Scott, R. C., Leedy, K. D., Bayraktaroglu, B., Look, D. C. & Zhang, Y.-H. Highly conductive ZnO grown by pulsed laser deposition in pure Ar. *Applied Physics Letters* **97**, 072113-072113 (2010).
- 91 Look, D. C. Recent advances in ZnO materials and devices. *Materials Science and Engineering: B* **80**, 383-387, doi:[http://dx.doi.org/10.1016/S0921-5107\(00\)00604-8](http://dx.doi.org/10.1016/S0921-5107(00)00604-8) (2001).
- 92 Kim, D.-H., Park, M.-R., Lee, H.-J. & Lee, G.-H. Thickness dependence of electrical properties of ITO film deposited on a plastic substrate by RF magnetron sputtering. *Applied Surface Science* **253**, 409-411, doi:<http://dx.doi.org/10.1016/j.apsusc.2005.12.097> (2006).

- 93 Suzuki, A. *et al.* Ultrathin Al-doped transparent conducting zinc oxide films fabricated by pulsed laser deposition. *Thin Solid Films* **517**, 1478-1481, doi:<http://dx.doi.org/10.1016/j.tsf.2008.09.024> (2008).
- 94 Lee, M.-J., Lim, J., Bang, J., Lee, W. & Myoung, J.-M. Effect of the thickness and hydrogen treatment on the properties of Ga-doped ZnO transparent conductive films. *Applied Surface Science* **255**, 3195-3200, doi:<http://dx.doi.org/10.1016/j.apsusc.2008.09.023> (2008).
- 95 Minami, T., Miyata, T., Ohtani, Y. & Kuboi, T. Effect of thickness on the stability of transparent conducting impurity-doped ZnO thin films in a high humidity environment. *physica status solidi (RRL) – Rapid Research Letters* **1**, R31-R33, doi:[10.1002/pssr.200600009](https://doi.org/10.1002/pssr.200600009) (2007).
- 96 Look, D. C., Leedy, K. D., Tomich, D. H. & Bayraktaroglu, B. Mobility analysis of highly conducting thin films: Application to ZnO. *Applied Physics Letters* **96**, 062102-062103 (2010).
- 97 Look, D. C. *et al.* Model for thickness dependence of mobility and concentration in highly conductive zinc oxide. *OPTICE* **52**, 033801-033801, doi:[10.1117/1.oe.52.3.033801](https://doi.org/10.1117/1.oe.52.3.033801) (2013).
- 98 Karlsson, B., Shimshock, R. P., Seraphin, B. O. & Haygarth, J. C. Optical properties of CVD-coated TiN, ZrN and HfN. *Solar Energy Materials* **7**, 401-411, doi:[http://dx.doi.org/10.1016/0165-1633\(83\)90013-8](http://dx.doi.org/10.1016/0165-1633(83)90013-8) (1983).
- 99 Itagaki, N., Kuwahara, K., Matsushima, K. & Oshikawa, K. 826306-826306-826306.
- 100 Itagaki, N. *et al.* Highly Conducting and Very Thin ZnO:Al Films with ZnO Buffer Layer Fabricated by Solid Phase Crystallization from Amorphous Phase. *Applied Physics Express* **4**, 011101 (2011).
- 101 Itagaki, N., Kuwahara, K., Matsushima, K. & Oshikawa, K. in *Proc. SPIE 8263, Oxide-based Materials and Devices III*. 826306.
- 102 Kuwahara, K. *et al.* High quality epitaxial ZnO films grown on solid-phase crystallized buffer layers. *Thin Solid Films* **520**, 4674-4677, doi:<http://dx.doi.org/10.1016/j.tsf.2011.10.136> (2012).
- 103 Look, D. C. Two-layer Hall-effect model with arbitrary surface-donor profiles: application to ZnO. *Journal of Applied Physics* **104**, 063718-063717 (2008).
- 104 Look, D. C., Droubay, T. C. & Chambers, S. A. Stable highly conductive ZnO via reduction of Zn vacancies. *Applied Physics Letters* **101**, 102101-102103 (2012).
- 105 Look, D. C. *et al.* Self-compensation in semiconductors: The Zn vacancy in Ga-doped ZnO. *Physical Review B* **84**, 115202 (2011).
- 106 Allen, M. S., Allen, J. W., Wenner, B. R., Look, D. C. & Leedy, K. D. in *Proc. SPIE 8626, Oxide-based Materials and Devices IV*. 862605 (2013).
- 107 Allen, M. S., Allen, J. W., Wenner, B. R., Look, D. C. & Leedy, K. D. Application of highly conductive ZnO to the excitation of long-range plasmons in symmetric hybrid waveguides. *OPTICE* **52**, 064603, doi:[10.1117/1.oe.52.6.064603](https://doi.org/10.1117/1.oe.52.6.064603) (2013).
- 108 Zia, R., Selker, M. D. & Brongersma, M. L. Leaky and bound modes of surface plasmon waveguides. *Physical Review B* **71**, 165431 (2005).
- 109 Berini, P. Figures of merit for surface plasmon waveguides. *Opt. Express* **14**, 13030-13042 (2006).
- 110 Ditlbacher, H. *et al.* Coupling dielectric waveguide modes to surface plasmon polaritons. *Opt. Express* **16**, 10455-10464 (2008).

- 111 Guo, X. *et al.* Direct Coupling of Plasmonic and Photonic Nanowires for Hybrid Nanophotonic Components and Circuits. *Nano Letters* **9**, 4515-4519, doi:10.1021/nl902860d (2009).
- 112 Wirth, J. C., Wenner, B. R., Allen, M. S., Allen, J. W. & Qi, M. 857001-857001-857007.
- 113 Yoshie, T., Tang, L. & Su, S.-Y. Optical Microcavity: Sensing down to Single Molecules and Atoms. *Sensors* **11**, 1972-1991 (2011).
- 114 Jokerst, N. *et al.* Chip scale integrated microresonator sensing systems. *Journal of Biophotonics* **2**, 212-226, doi:10.1002/jbio.200910010 (2009).
- 115 Zia, R., Schuller, J. A. & Brongersma, M. L. Near-field characterization of guided polariton propagation and cutoff in surface plasmon waveguides. *Physical Review B* **74**, 165415 (2006).
- 116 Lal, S., Link, S. & Halas, N. J. Nano-optics from sensing to waveguiding. *Nat Photon* **1**, 641-648 (2007).
- 117 Lawandy, N. M. Localized surface plasmon singularities in amplifying media. *Applied Physics Letters* **85**, 5040-5042 (2004).
- 118 Sudarkin, A. N. & Demkovich, P. A. Excitation of surface electromagnetic waves on the boundary of a metal with an amplifying medium. *Soviet Physics - Technical Physics* **34**, 764-766 (1989).
- 119 Hosseini, A. & Massoud, Y. Nanoscale surface plasmon based resonator using rectangular geometry. *Applied Physics Letters* **90**, 181102-181103 (2007).
- 120 Grandidier, J. *et al.* Gain-Assisted Propagation in a Plasmonic Waveguide at Telecom Wavelength. *Nano Letters* **9**, 2935-2939, doi:10.1021/nl901314u (2009).
- 121 Maier, S. A. Gain-assisted propagation of electromagnetic energy in subwavelength surface plasmon polariton gap waveguides. *Optics Communications* **258**, 295-299, doi:<http://dx.doi.org/10.1016/j.optcom.2005.07.064> (2006).
- 122 Nezhad, M., Tetz, K. & Fainman, Y. Gain assisted propagation of surface plasmon polaritons on planar metallic waveguides. *Opt. Express* **12**, 4072-4079 (2004).
- 123 Seidel, J., Grafström, S. & Eng, L. Stimulated Emission of Surface Plasmons at the Interface between a Silver Film and an Optically Pumped Dye Solution. *Physical Review Letters* **94**, 177401 (2005).
- 124 Noginov, M. A. *et al.* Enhancement of surface plasmons in an Ag aggregate by optical gain in a dielectric medium. *Optics Letters* **31**, 3022-3024 (2006).
- 125 Lorenz, M. *et al.* Optical and electrical properties of epitaxial  $(\text{Mg},\text{Cd})_x\text{Zn}_{1-x}\text{O}$ ,  $\text{ZnO}$ , and  $\text{ZnO}:(\text{Ga},\text{Al})$  thin films on c-plane sapphire grown by pulsed laser deposition. *Solid-State Electronics* **47**, 2205-2209, doi:[http://dx.doi.org/10.1016/S0038-1101\(03\)00198-9](http://dx.doi.org/10.1016/S0038-1101(03)00198-9) (2003).
- 126 Pearton, S. J., Norton, D. P., Ip, K., Heo, Y. W. & Steiner, T. Recent progress in processing and properties of  $\text{ZnO}$ . *Progress in Materials Science* **50**, 293-340, doi:<http://dx.doi.org/10.1016/j.pmatsci.2004.04.001> (2005).
- 127 West, P. R. *et al.* Searching for better plasmonic materials. *Laser & Photonics Reviews* **4**, 795-808, doi:10.1002/lpor.200900055 (2010).
- 128 Dionne, J. A., Diest, K., Sweatlock, L. A. & Atwater, H. A. PlasMOStor: A Metal–Oxide–Si Field Effect Plasmonic Modulator. *Nano Letters* **9**, 897-902, doi:10.1021/nl803868k (2009).

- 129 Oubre, C. & Nordlander, P. Optical Properties of Metallodielectric Nanostructures Calculated Using the Finite Difference Time Domain Method. *The Journal of Physical Chemistry B* **108**, 17740-17747, doi:10.1021/jp0473164 (2004).
- 130 Veronis, G. & Fan, S. Theoretical investigation of compact couplers between dielectric slabwaveguides and two-dimensional metal-dielectric-metal plasmonicwaveguides. *Opt. Express* **15**, 1211-1221 (2007).
- 131 van Wijngaarden, J. T. *et al.* Direct imaging of propagation and damping of near-resonance surface plasmon polaritons using cathodoluminescence spectroscopy. *Applied Physics Letters* **88**, 221111-221113 (2006).
- 132 Allione, M., Temnov, V. V., Fedutik, Y., Woggon, U. & Artemyev, M. V. Surface Plasmon Mediated Interference Phenomena in Low-Q Silver Nanowire Cavities. *Nano Letters* **8**, 31-35, doi:10.1021/nl071763o (2007).
- 133 Volkov, V. S., Bozhevolnyi, S. I., Devaux, E., Laluet, J.-Y. & Ebbesen, T. W. Wavelength Selective Nanophotonic Components Utilizing Channel Plasmon Polaritons. *Nano Letters* **7**, 880-884, doi:10.1021/nl070209b (2007).
- 134 Xiao, S., Liu, L. & Qiu, M. Resonator channel drop filters in a plasmon-polaritons metal. *Opt. Express* **14**, 2932-2937 (2006).
- 135 Zia, R., Schuller, J. A., Chandran, A. & Brongersma, M. L. Plasmonics: the next chip-scale technology. *Materials Today* **9**, 20-27, doi:[http://dx.doi.org/10.1016/S1369-7021\(06\)71572-3](http://dx.doi.org/10.1016/S1369-7021(06)71572-3) (2006).
- 136 Boltasseva, A. *et al.* Integrated Optical Components Utilizing Long-Range Surface Plasmon Polaritons. *J. Lightwave Technol.* **23**, 413 (2005).